Science and Technology of
Advanced Materials

TOPICAL REVIEW

Active nanocharacterization of nanofunctional materials by scanning tunneling microscopy

IOP PUBLISHING SCIENCE AND TECHNOLOGY OF ADVANCED MATERIALS

Sci. Technol. Adv. Mater. **9** (2008) 013003 (9pp) doi:10.1088/1468-6996/9/1/013003

TOPICAL REVIEW

Active nanocharacterization of nanofunctional materials by scanning tunneling microscopy

Daisuke Fujita and Keisuke Sagisaka

Advanced Nano Characterization Center, National Institute for Materials Science, 1-2-1 Sengen, Tsukuba 305-0047, Japan

E-mail: fujita.daisuke@nims.go.jp

Received 22 June 2007
Accepted for publication 9 October 2007
Published 13 March 2008
Online at stacks.iop.org/STAM/9/013003

Abstract

Recent developments in the application of scanning tunneling microscopy (STM) to nanofabrication and nanocharacterization are reviewed. The main focus of this paper is to outline techniques for depositing and manipulating nanometer-scale structures using STM tips. Firstly, the transfer of STM tip material through the application of voltage pulses is introduced. The highly reproducible fabrication of metallic silver nanodots and nanowires is discussed. The mechanism is thought to be spontaneous point-contact formation caused by field-enhanced diffusion to the apex of the tip. Transfer through the application of *z*-direction pulses is also introduced. Sub-nanometer displacement pulses along the *z*-direction form point contacts that can be used for reproducible nanodot deposition. Next, the discovery of the STM structural manipulation of surface phases is discussed. It has been demonstrated that superstructures on Si(001) surfaces can be reverse-manipulated by controlling the injected carriers. Finally, the fabrication of an atomic-scale one-dimensional quantum confinement system by single-atom deposition using a controlled point contact is presented. Because of its combined nanofabrication and nanocharacterization capabilities, STM is a powerful tool for exploring the nanotechnology and nanoscience fields.

Keywords: nanotechnology, nanocharacterization, scanning tunneling microscopy, scanning probe microscopy, nanomaterials, nanofabrication

(Some figures in this article are in colour only in the electronic version.)

1. Introduction

With the recent trend of miniaturization in electronics, magnetic devices, and nano electro-mechanical systems (NEMS), materials science researchers are now frequently confronted with nanostructured materials on a scale below ∼100 nm [1]. It is well known that nanotechnology-driven materials research, or nanotechnology-assisted materials research, plays a key role both in basic science and in industrial innovations of novel nanometer-scale products such as nanoelectronics devices. The development of advanced fabrication and characterization technologies for novel nanofunctional materials is one of the most important subjects in advanced nanomaterials research. Since the dimensions of novel microscopic devices will shrink to true nanometer scale below ∼10 nm in the near future, the development of a probe for fabrication and *in situ* characterization at true nanometer scale is urgently needed. Moreover, the merging of nanofabrication and nanocharacterization tools into a unified tool will enhance the productivity of nanomaterials

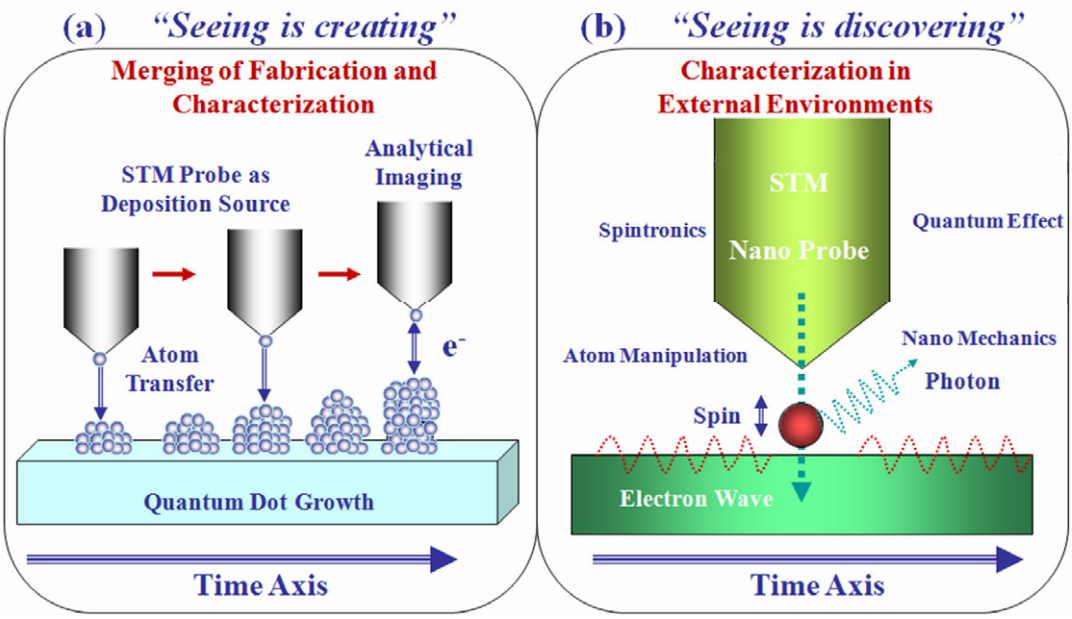

Figure 1. Active nanocharacterization using STM. (a) In the 'seeing is creating' type, nanofabrication and nanocharacterization are merged. (b) The 'seeing is discovering' type involves dynamic characterization in externally applied fields or environments.

processing. The idea of 'active nanocharacterization' has been proposed with the aim of making this merging of tools a reality [2, 3]. Active nanocharacterization is defined as the nanometer-scale dynamic characterization with applied operations or environments that are closely related to actual nanofabrication processing or nanofunctionality working conditions.

Among the various nanometer-scale analysis techniques, scanning tunneling microscopy (STM) is one of the best candidate techniques for active nanocharacterization. First, STM can depict the true atomic resolution of a single atom on various conductive surfaces [4]. In contrast, a transmission electron microscope (TEM) can resolve an individual atomic column but cannot probe a single atom or molecule on a surface. Moreover, STM has the unique capability of locally probing electronic states, which are closely related to novel nanofunctionality. For example, STM with tunneling spectroscopy can be used to perform atomically resolved spectroscopy imaging functions such as energy-resolved local density of states (LDOS) mapping [5], spin-polarized tunneling imaging [6], molecular vibrational spectroscopy by inelastic tunneling [7], and tunneling-induced photon emission mapping [8]. This versatility as an analytical probe makes STM a powerful tool for exploring novel properties and the innovative functions of nanomaterials.

STM has also demonstrated another type of versatility as a nanofabrication tool, performing functions including atom manipulation [9], local deposition by the decomposition of organometallic gases [10], local selective oxidation [11], nanometer-scale lithography [12], and local deposition by the electric-field-induced transfer of tip atoms [13]. Moreover, STM can be adapted to various environments such as air, ultrahigh vacuum (UHV), controlled atmospheres and liquid. Thus, it is clear that STM has great potential as a highly versatile tool for nanofabrication and nanocharacterization in various environments, that is, for active nanocharacterization. Two major categories of active nanocharacterization using STM are shown schematically in figure 1. One is the so-called 'seeing is creating' type, where nanofabrication and nanocharacterization are merged into a continuous process. A typical example is quantum dot fabrication by tip-material transfer and the subsequent analysis of electronic properties. The other is the so-called 'seeing is discovering' type, where dynamic characterization under externally applied fields or environments is performed to discover novel nanofunctionality or to clarify the mechanism of the nanofabrication process.

Here, recent developments in nanofabrication and nanocharacterization technology using STM are reviewed. First, two novel STM nanofabrication methods using tip-material transfer are introduced. Then the discovery of the STM manipulation of surface phases induced by carrier injection is discussed. Finally, the fabrication of an atomic-scale one-dimensional (1D) system using a single-atom-transfer technique with a controlled point contact is demonstrated. Because of its combination of nanofabrication and nanocharacterization capabilities, STM is a powerful tool for exploring the nanotechnology and nanoscience fields.

2. Nanostructure fabrication by tip-material transfer using voltage pulses

Conductive nanostructures such as nanodots and nanowires are important building blocks for composing nanodevices. In fact, these metallic nanostructures themselves are also research targets of nanoscience because their nanometer-scale size and low dimensionality may create novel quantum effects. One goal of nanotechnology-driven materials research is to fabricate nanometer-scale devices with functions superior

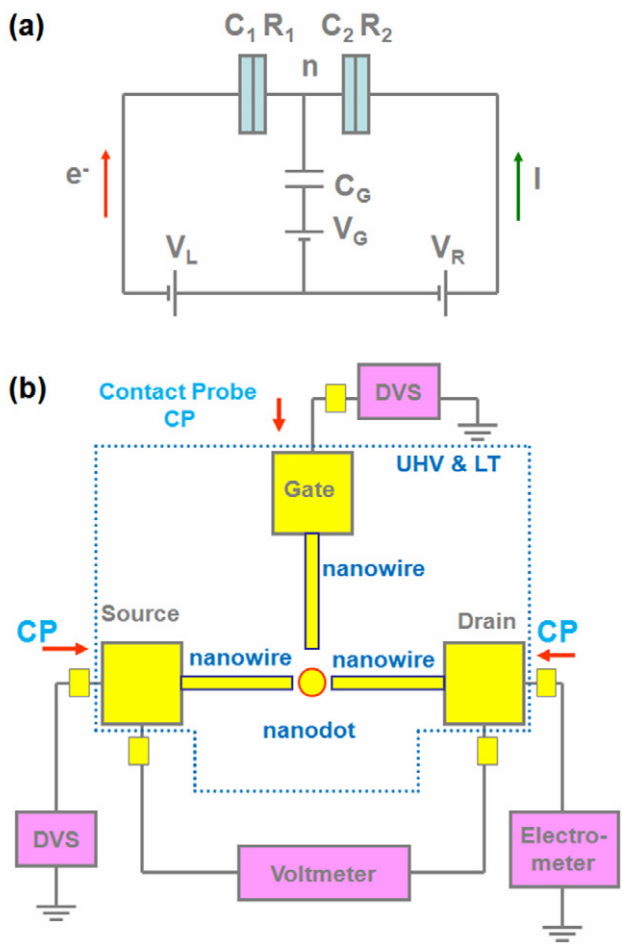

Figure 2. (a) Schematic circuit diagram of a SET transistor. (b) Schematic representation of a nanometer-scale SET transistor in UHV. To fabricate a SET nanodevice, novel techniques for fabricating nanometer-scale circuit parts such as nanowires and nanodots on semiconductor substrates should be developed.

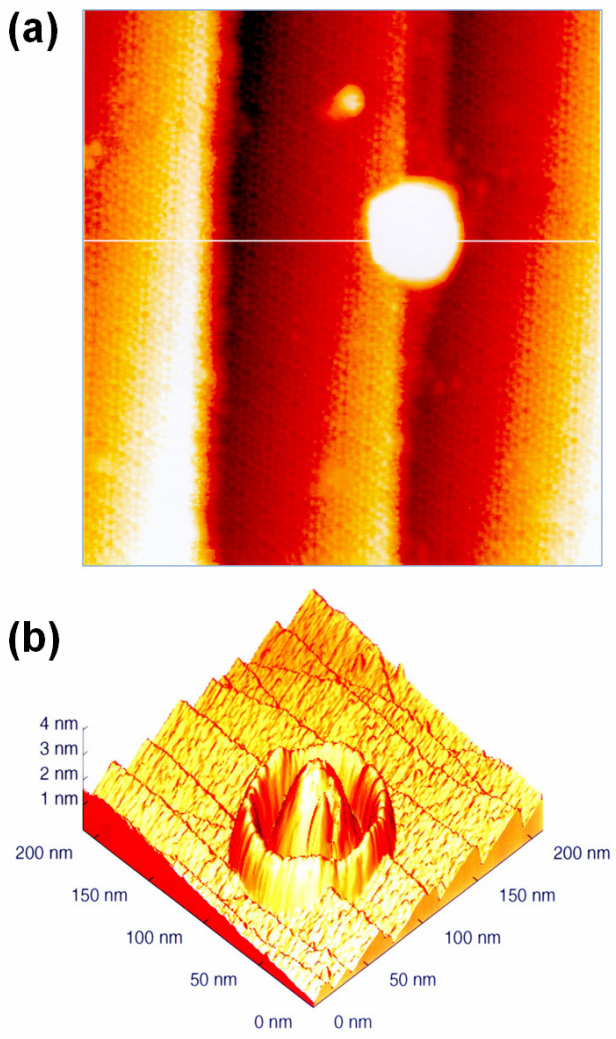

Figure 3. (a) STM image of atomically resolved Si(111) surface in UHV after applying a negative voltage pulse ($V_{tip} = -5.0$ V, $T_{pulse} = 5$ ms) to a gold-coated tungsten tip. A gold nanomound (10 nm ϕ, 1 nm high) was formed on a step where the electric field is strongest. (b) STM image of a gold nanodot obtained after applying a positive voltage pulse ($V_{tip} = +8.0$ V, $T_{pulse} = 1$ ms).

to those of conventional microelectronics devices. For example, a nanometer-scale circuit composed of conductive nanowires, tunneling barriers, and a conductive nanodot has a single-electron tunneling (SET) effect, which can be applied to the fabrication of microscopic transistors and memories [14]. A nanometer-scale SET transistor, an important candidate technology for high-speed, low-power large-scale integrated circuits (LSIs), is schematically shown in figure 2. To develop such nanodevices, reproducible nanofabrication techniques for the fabrication of metallic nanostructures on clean substrates must first be developed.

Although conventional methods of fabricating artificial metallic nanostructures are mainly based on electron-beam lithography (EBL) [15], various STM-based methods have been developed due to the versatility of STMs [9–13]. One of the most intensively investigated STM-based nanofabrication techniques is the electric-field-induced material transfer of a tip to a substrate through the application of voltage pulses [16–29]. Because the pulse width applied is less than ∼1 ms, this method is fast. Mamin *et al* [13] were the first to demonstrate the electric-field-induced deposition of tip materials in 1990. They demonstrated that atomic emission from a gold tip to a gold substrate through the application of voltage pulses in air can be used to write gold nanodot patterns with no apparent degradation of the tip. During the early 1990s, many researchers reported the field-induced transfer of tip materials through the application of voltage pulses in various environments, such as in air [16–19], UHV [20, 21], or liquid [22]. By these tip-material-transfer methods, various sizes of nanomounds can in principle be deposited at the desired position. However, atomic-resolution STM imaging with a tip used for field-induced deposition was not achieved until 1996.

In 1996, Fujita *et al* [23] demonstrated the field-induced deposition of gold nanodots on an atomically resolved Si(111)-(7 × 7) surface using a gold-coated tip in UHV. Typical STM images of gold nanostructures fabricated at room temperature (RT) are shown in figure 3. Gold nanodots ∼10 nm in diameter and ∼1 nm in height were deposited by applying a single negative voltage pulse

to a gold-coated tungsten tip, as shown in figure 3(a). In contrast, upon applying a voltage pulse with positive polarity to the tip, a larger nanomound, typically ∼50 nm in diameter and ∼3 nm in height, was deposited, as shown in figure 3(b). Only with a negative polarity tip was deposition controllable and the fabrication of an arbitrary pattern of gold nanodots in accordance with a specified design possible. The threshold voltage for gold atom transfer is approximately ∼5 V. The corresponding electric field of $\sim 5\,\mathrm{V\,nm^{-1}}$ is significantly lower than the reported threshold value for the field evaporation of Au^- ($\sim 17\,\mathrm{V\,nm^{-1}}$) [30]. Although the deposition of gold nanodots on clean Si surfaces in UHV was successfully demonstrated by applying voltage pulses and has been extensively studied [24, 29], the formation of continuous nanowires was found to be difficult due to the low deposition probability of gold (∼60%) [23].

An STM tip-material transfer study on a new material (silver), in which metallic nanodots on a clean Si(111) surface were obtained with much higher reproducibility, was recently reported [28]. The STM tip was made of an electrochemically etched tungsten wire (99.99% purity) on which a thin silver film was deposited by magnetron sputtering. Although it was possible to transfer silver at both polarities, a negative polarity was again found to be more suitable for nanofabrication because of the higher probability of deposition (up to 100%) and smaller nanodot dimensions. The observed threshold voltage for negative polarity is about 3.5 V, which is significantly smaller than that for gold. Above the threshold, the deposition probability reaches ∼100%. Figure 4(a) shows an STM image of silver nanodots after applying several voltage pulses. Its line profile, as shown in figure 4(b), clearly indicates that the nanometer-scale dots can be created with a relatively small voltage. Owing to the nearly perfect deposition yield, nanodots, nanowires and nanocharacters can be created, as shown in figure 4(c), demonstrating the versatility of STM tip-material transfer for developing nanometer-scale circuits. Tunneling spectroscopy performed above a silver nanodot showed linear *I–V* characteristics around zero bias indicating a metallic nature. *I–V* curves observed above the neighboring silver nanodots showed that there was a decrease in tunneling current, indicating the presence of a carrier depletion layer. If a high-work-function metal comes in contact with an n-type semiconductor, electrons flow from the semiconductor to the metal, depleting the characteristic surface region of the semiconductor of electrons. Consequently, local electrical resistivity increases near the surface with respect to its bulk value. Similar space-charge regions under gold nanodots on n-Si(111) were also demonstrated by artificial point contact [31].

Despite these extensive studies on field-induced tip-material transfer, no consensus regarding the mechanism of nanodot deposition by applying voltage pulses has been reached. Generally, the proposed models can be categorized into two types. One is the field evaporation model [13, 16, 18–21, 26, 27], and the other is the mechanical point-contact model [17, 22, 25, 28, 29]. The combination of field evaporation and mechanical point contact has also been proposed [23]. The field evaporation model was first proposed by Mamin *et al* [13] in the case of atom emission from a gold tip on a Au(111) surface in air. A detailed physical

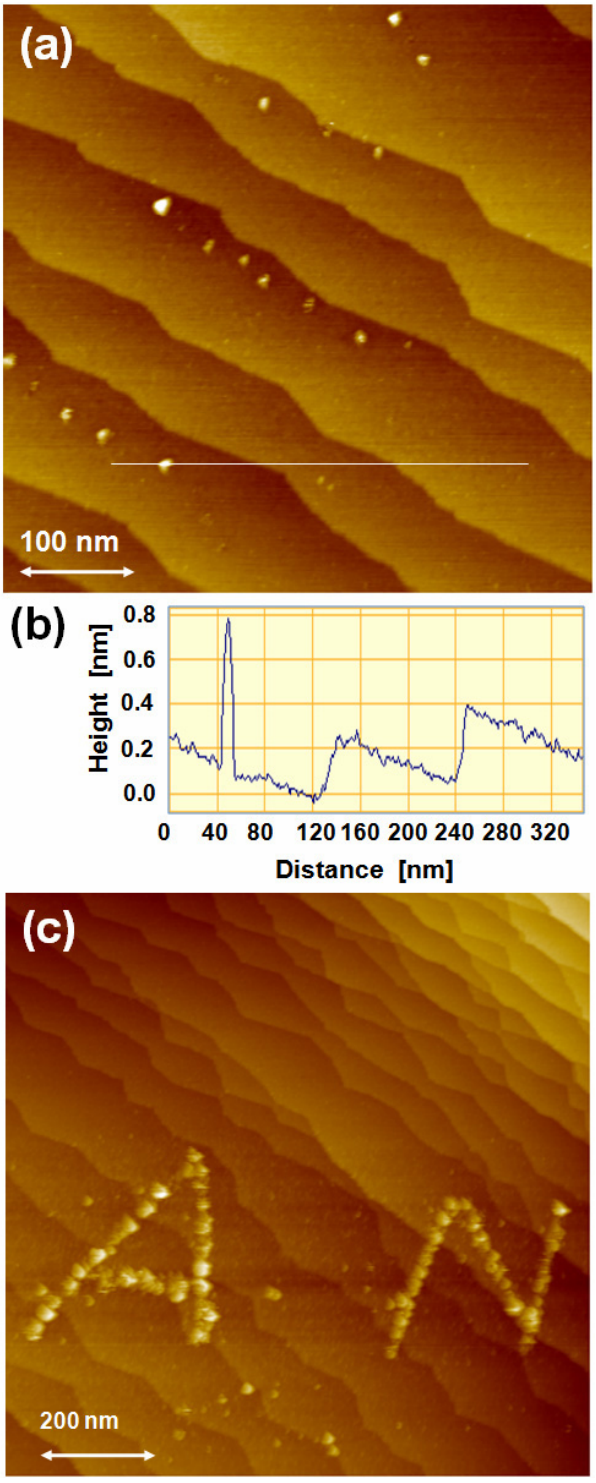

Figure 4. (a) STM image of silver nanodots on Si(111) surface after applying a negative voltage pulse ($V_{tip} = -3.5$ V, $T_{pulse} =$ 1 ms) to a silver-coated tungsten tip. (b) Profile along line indicated in (a), showing the formation of a silver nanodot (height = 0.7 nm, diameter = 8.0 nm at half maximum). (c) STM image of silver nanocharacters 'A' and 'N' created by applying negative voltage pulses ($V_{tip} = -4.5$ V, $T_{pulse} = 1$ ms).

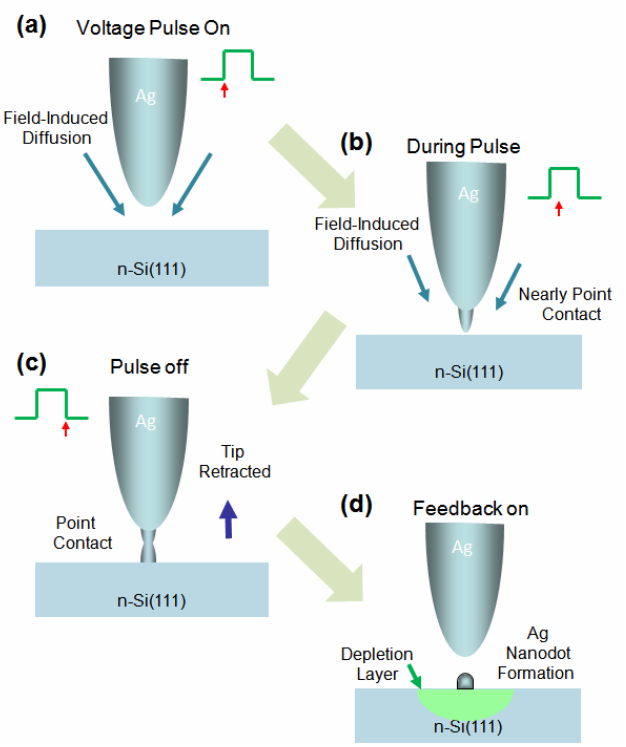

Figure 5. Schematic model of tip-material transfer mechanism from an Ag tip to n-Si(111) by applying a negative voltage pulse. (a) A negative voltage pulse is applied, causing field-induced diffusion of Ag towards the apex of the tip. (b) The elongated tip apex may cause a spontaneous point contact during the pulse. (c) Immediately after the pulse ends, feedback is recovered, causing the tip to retract and the point contact to break. (d) Because of the relatively strong chemical bond, a metallic Ag nanodot is left, forming a nearby depletion layer.

model of the field evaporation of atoms from various STM tip materials was proposed by Tsong [30]. The mechanical point-contact model was first proposed by Pascual *et al* [17] for a Au tip/Au substrate system. The observed quantization of current flowing between the Au tip and the Au substrate seems to be direct evidence of point-contact formation. Huang *et al* [25] explained the formation of Pt nanodots on a Si(111) surface using a Pt tip as being due to atomic point contact. They measured the tip displacement and the current through the tip during the formation of nanodots to show that point contacts were formed during the voltage pulses.

Although several researchers explained the tip-material transfer through the application of voltage pulses as being due to field evaporation, it is unlikely to occur in the case of silver because the threshold field for the field evaporation ($\sim$22 V nm^{-1}) of Ag^{-} at negative polarity [30] is significantly larger than the observed threshold field for tip-material transfer ($\sim$3.5 V nm^{-1}) [28]. Therefore, negative voltage pulses are unlikely to cause field evaporation in the case of Ag nanodot deposition. Our model for tip-material transfer from a silver tip to an n-Si(111) surface is shown in figure 5, which is based on spontaneous point-contact formation. First, the tip is located at a height regulated by feedback control, which is typically $\sim$1 nm, depending on the tunneling conditions. Then, the feedback control is turned off and a voltage pulse is applied to the tip. During the pulse, an increase in tunneling current is usually observed, indicating a decrease in gap distance due to the elongation of the silver tip. When the gap distance approaches the atomic distance, a nanometer-scale point contact is spontaneously formed. This can be confirmed by an abrupt jump in current to $\sim\mu$A order. The most probable mechanism for tip elongation is nanoprotrusion formation by the field-enhanced diffusion of silver to the apex of the tip. It is well known that a high electric field causes atoms at the tip shank to diffuse to the apex by field-gradient-induced surface diffusion [30]. After the tip is retracted, a nanometer-scale silver mound is left on the surface because of the relatively strong chemical bonding between silver and silicon atoms.

3. Nanostructure fabrication by tip-material transfer using *z*-direction pulses

The voltage pulse method described above is suitable for fabricating nanodots of various dimensions. If tip-material transfer is mainly caused by the spontaneous formation of a point contact, then it will be possible to deposit the tip material by artificial point-contact formation. On the basis of this idea, the so-called '*z*-pulse method' was developed [31]. This technique uses the controlled approach of the tip to the surface to form an atomic point contact by applying a voltage pulse to a *z*-direction piezo-actuator. An example of tip-material transfer using the *z*-pulse method with a pure gold tip is given here.

When a small *z*-axis-displacement pulse (Δz) corresponding to a tunneling gap distance of less than 1 nm is applied to a gold tip located in the tunneling region, a gold nanodot can be formed on the surface under certain conditions, as shown schematically in figure 6(a). In the initial stage, the tip is located at a regulated height. The gap distance is typically approximately 0.5 nm, depending on the tunneling conditions, such as applied gap voltage and feedback current. By applying a *z*-pulse, the gold tip typically approaches to within $\sim$0.3 nm of the surface. When the gap distance is close to a typical bond length of $\sim$0.2 nm, an atomic-sized point contact is spontaneously formed by the formation of an atomic-scale protrusion, which may be caused by field-induced diffusion or by the formation of a chemical bond. According to the dimer–adatom–stacking-fault (DAS) model, the Si(111)-(7$\times$7) surface contains surface adatoms, which have dangling bonds protruding into the vacuum [32]. Therefore, it is possible to form an atomic-sized point contact through chemical bonding with these dangling bonds if the gap distance is sufficiently small for both wave functions to overlap. After extracting the tip, because of the chemical bonds between the gold and silicon atoms a nanoscale gold dot is left on the surface.

An image of a typical gold nanodot formed after applying a single *z*-pulse ($\Delta z = -0.3$ nm, $T_{\mathrm{pulse}} = 1$ ms) at 50 K [31] is shown in figure 6(b). The image clearly shows a gold nanodot protruding from the Si(111)-(7$\times$7) surface, whose dimensions are about 6 nm in diameter across the base and 0.9 nm in height. Compared with the voltage pulse method, the advantage of the *z*-pulse method is its higher deposition

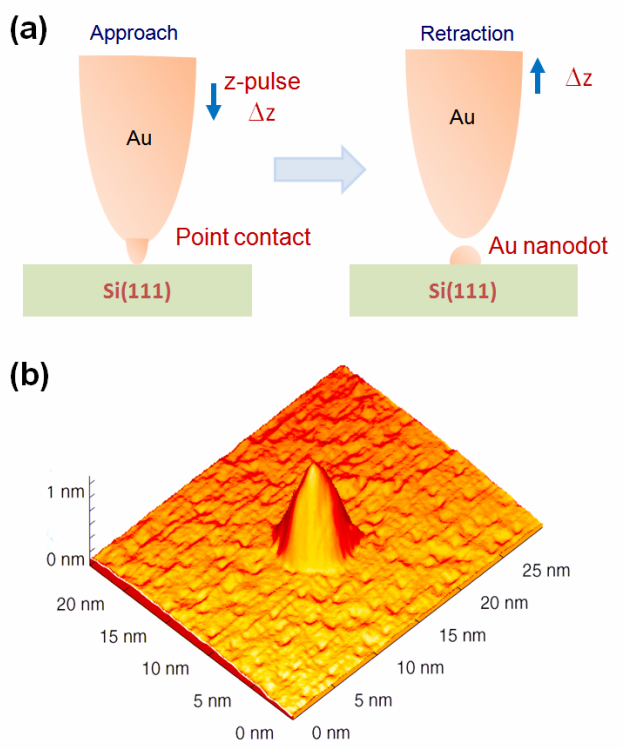

Figure 6. (a) Schematic representation of tip-material transfer from a gold tip to a Si(111) surface by the spontaneous formation of a point contact by applying a single *z*-pulse. (b) STM image of a gold nanodot formed on a Si(111)-(7×7) surface after applying a single *z*-pulse ($\Delta z = -0.3$ nm, $T_p = 1$ ms) to a gold tip at 50 K.

probability. If tip conditions, such as the shape of the apex, are suitable, a gold nanodot almost always forms after a single *z*-pulse is applied.

By measuring the gap current between the gold tip and the Si(111) surface against the change in the gap distance (*I*–*z* curve), it is possible to demonstrate that the tip-material transfer is actually caused by point-contact formation. Figure 7 shows a typical *I*–*z* curve obtained at RT. To measure the current flow, a small constant voltage V_t was applied to the tip. At first the observed current showed an exponential increase because the tip was still in the tunneling regime. At approximately −0.2 nm closer to the surface than the regulated position, the current suddenly jumped to a much higher value (about 25 nA), after which the current was almost constant up to −0.3 nm. This discrete change in current clearly suggests the formation of a point contact between the gold tip and the Si(111) surface. Point-contact formation using an STM configuration has been studied for various metal surfaces (Au, Ni, Cu, Pt, Al) [17, 33–35], and the conductance G showed jumps of multiples of $2e^2/h (=77.5\mu S)$ as the contact was stretched. Using the Landauer–Büttiker formula, the quantum conductance of a nanowire can be expressed as

$$G = \frac{2e^2}{h} \sum_{i=1}^{N_C} T_i \qquad (1)$$

where N_C is the number of conduction channels supported by the point contact and T_i is the transmission probability of the

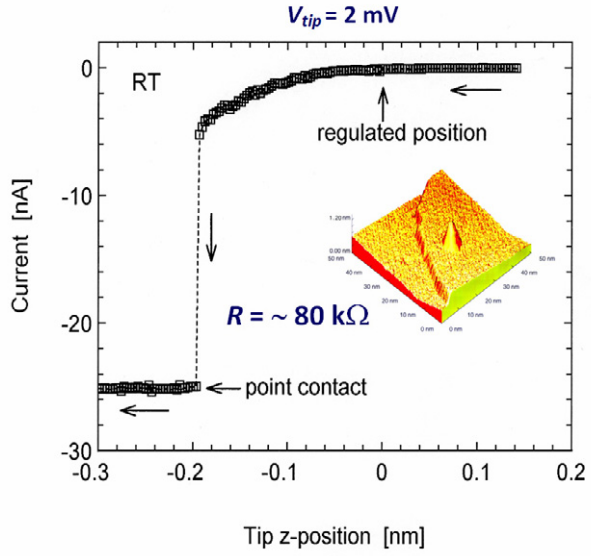

Figure 7. Current–distance (*I*–*z*) curve obtained on Si(111)-(7×7) surface at RT. During measurement, a small voltage was applied to a gold tip ($V_t = 2$ mV). Insert: STM image observed after *I*–*z* curve measurement.

*i*th channel. If a point contact with a few channels forms and the transmission probability is unity ($T_i = 1$), then the contact resistance should show a quantized value $R_c = R_Q/N_c$, where quantum resistance R_Q is defined as $h/2e^2 (=12.9\,\text{k}\Omega)$. The total resistance R_{total} at the observed current plateau in figure 7 is about 80 kΩ, which is on the same order as the quantized resistance. Therefore, the observed jump in the *I*–*z* curve can be partially attributed to a consequence of the quantized conductance, which suggests that a nanometer-scale point contact was formed between the gold tip and the Si(111) surface. The significant deviation from R_c can be explained by the spontaneous formation of a depletion region underneath the contact and by the relatively large reflection caused by the mismatch of Fermi wavenumbers in the two media.

The insert in figure 7 is an STM image taken immediately after *I*–*z* curve measurement and clearly shows the formation of a gold nanodot. Its size is about the same as that obtained by the single *z*-pulse shown in figure 6, which suggests that nanodot formation by tip-material transfer is caused by the formation of a nanoscale point contact.

4. STM phase manipulation by carrier injection

The Si(001) wafer is the most important material in semiconductor technology. Although its surface structure has been extensively studied for decades, the ground state of the Si(001) surface at low temperatures was not clearly understood until recently. Since uncertainty about the ground state of such an important material may have a significant effect on the development of precise simulation methods of semiconductor processing, research in this area should be of the highest priority.

With the rapid development of low-temperature UHV–STM, various structures, such as static (2×1) [36], dynamic (2×1) [37, 38], p(2×2) [39], and c(4×2), have been

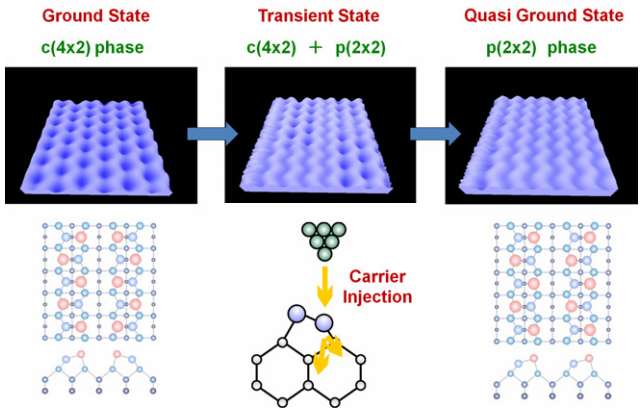

Figure 8. STM images showing STM manipulation of periodic superstructures on an n-type Si(001) surface at 5 K. A gradual increase in injected electron energy changes the surface superstructure from the ground state, c(4 × 2), through the transient state to the quasi-ground state, p(2 × 2).

proposed as the ground state of the Si(001) surface [40]. Here, the static (2×1) structure is composed of symmetric dimers. The dynamic (2×1) structure is thought to be composed of apparently symmetric dimers. This structure is normally observed at temperatures near RT and is composed of buckled dimers in fast flip–flop motion. Since the flip–flop motion is a thermally activated phenomenon, lowering the temperatures to ∼120 K freezes the motion and causes asymmetric dimer structures of p(2×2) or c(4×2) to appear. First, the static and dynamic symmetric dimer structures were ruled out for the Si(001) surface by precise STM and NC-AFM measurements at approximately 5 K [41, 42]. Very low temperature STM measurement (670 mK) [43] and a low-temperature LEED study performed by Mizuno *et al* [44] clearly showed that c(4×2) is the most stable ground state. This conclusion is consistent with the result of first-principles DFT calculation [45].

Sagisaka *et al* [40] discovered a new method of STM manipulation while investigating the ground state of the Si(001) surface. By controlling the energy of carriers injected by an STM tip, it is possible to reverse-manipulate periodic surface superstructures at temperatures below ∼40 K [46]. As shown in figure 8, it is possible to manipulate the Si(001) surface phase between c(4×2) and p(2×2) by precisely controlling the sample bias in STM at such low temperatures. When the surface is scanned at a relatively low positive bias, it shows a single c(4×2) phase or the ground state. Gradually increasing the positive sample-bias voltage causes the surface dimer rows to fluctuate individually. This fluctuation was attributed to the flip-flop motion induced by the injected electrons. A further increase in the positive bias voltage caused the surface to shift to a single p(2×2) phase or to the quasi-ground state.

The reconstructed Si(001) surface exhibits low-dimensional surface electronic states originating from the dangling bonds of the dimer rows. The empty dangling bond state (π^*) is situated within the bulk band gap and reveals energy dispersion along the dimer-row direction. The filled dangling bond state (π) overlaps with the bulk valence band [47, 48]. Electron injection into the empty surface state (π^*) from the STM tip is responsible for the structural change from the ground state, c(4×2), to the quasi-ground state, p(2×2) [49]. In contrast, hole injection into the filled surface state (π) causes a structural change from the quasi-ground state, p(2×2), to the true ground state, c(4×2).

The observed structural manipulation by controlling the gap voltage provides a reasonable explanation as to why previous researchers reported different structures as the true ground state of the reconstructed Si(001) surface. Similar structural manipulation through STM carrier injection has been also discovered for Ge(001) surfaces at low temperatures by Takagi *et al* [50]. To obtain a unified mechanism for STM structural manipulation, further comparative studies between Si(001) and Ge(001) (with the help of theoretical modeling) should be carried out.

5. 1D quantum confinement by STM atom deposition using point contact

As described above, the reconstructed Si(001) surface at low temperatures exhibits interesting features such as a 1D electron state in which the surface electrons are preferably transported along individual dimer rows. The quantum interference of the 1D electron waves can be visualized by UHV–STM at low temperatures [51, 52]. Confinement of the 1D electrons using the dimer rows of the reconstructed Si(001) surface was first demonstrated by Yokoyama and Takayanagi [51], by evaporating aluminum onto the surface to form aluminum ad-dimer chains. These chains acted as potential barriers, confining 1D electron waves to along the dimer rows. The next challenge is to create artificially controlled structures at atomic scale to confine 1D electrons to a designed length along a single dimer row.

For this purpose, further improvement of the above-mentioned tip-material transfer technique by creating an artificial point contact between the STM tip and the surface is required. The obvious advantage of this method is that it enables the fabrication of atomic-scale scattering centers at desired positions. By transferring tungsten atoms from the STM tip of a sharpened tungsten wire, Sagisaka and Fujita have succeeded in fabricating a quasi-1D quantum well on a single dimer row [53]. Tungsten atoms were deposited through the formation of a point contact from the apex of a tip to the surface, as shown schematically in figure 9(a). Stable LT-STM operation in UHV is required for the reproducible positioning of the tip. The point contact was formed by moving the tip closer to the down atom of a buckled dimer. An STM image of a typical tungsten atom deposited on a Si(001) surface at 79 K is shown in figure 9(b). The observed protrusion in the center of the image is thought to be a tungsten atom deposited on the down atom of a buckled silicon dimer.

Using this atom deposition technique, the fabrication of two tungsten dots along a single dimer row with a suitable separation (∼10 nm) for effective quantum confinement was attempted, the result of which is shown in figure 10(a). If the tungsten atoms act as effective scattering

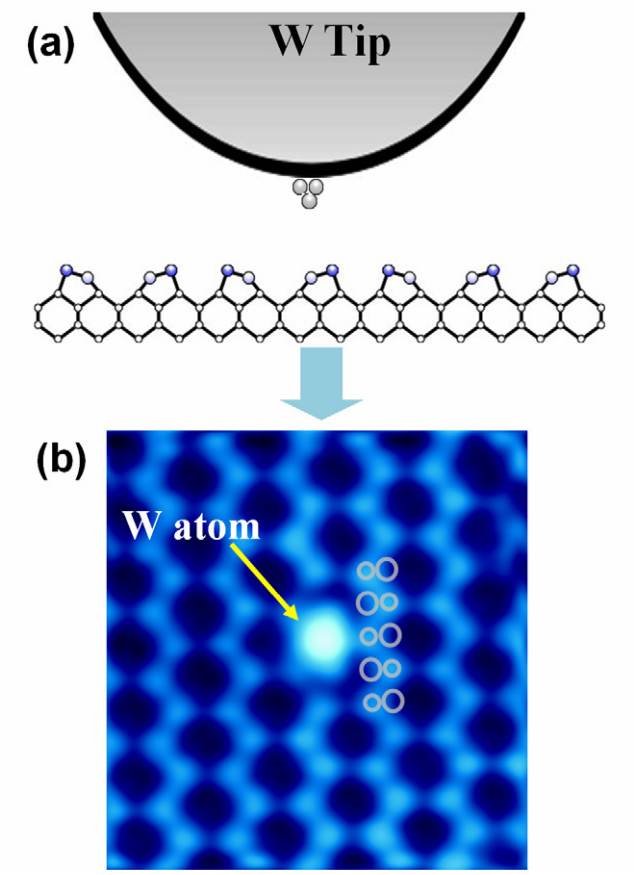

Figure 9. (a) Schematic representation of transfer of atom from tip to the down atom of a silicon dimer row by formation of artificial point contact. (b) STM image of a tungsten atom deposited on a reconstructed Si(001)-c(4×2) surface from STM tip at 79 K.

barriers to the dangling-bond-state (π^*) electrons, then the quasi-1D electron waves along the dimer row should be confined between the two scattering barriers, fully realizing an artificially fabricated 1D quantum well.

The LDOS at surfaces can be visualized by differential conductance ($\mathrm{d}I/\mathrm{d}V$) mapping using a lock-in technique. As shown in figure 10(b), the $\mathrm{d}I/\mathrm{d}V$ maps obtained from the dimer row with two tungsten dots clearly reveal confined electron waves. As the sample bias is increased, several quantized states are observed. This observation indicates that a single dimer row surrounded by two tungsten dots functions as a quasi-1D quantum well. These results clearly suggest that the STM atom deposition technique is compatible with high-resolution STM/STS imaging. The combination of fabrication and characterization techniques operable at atomic scale will further advance the exploration and clarification of novel quantum phenomena and functionalities.

6. Conclusion

Recent developments in nanofabrication and nanocharacterization technologies using STM were reviewed. Special emphasis was placed on the various fabrication techniques of nanometer-scale structures using STM tips acting as both nanofabrication and nanocharacterization tools. Firstly, an

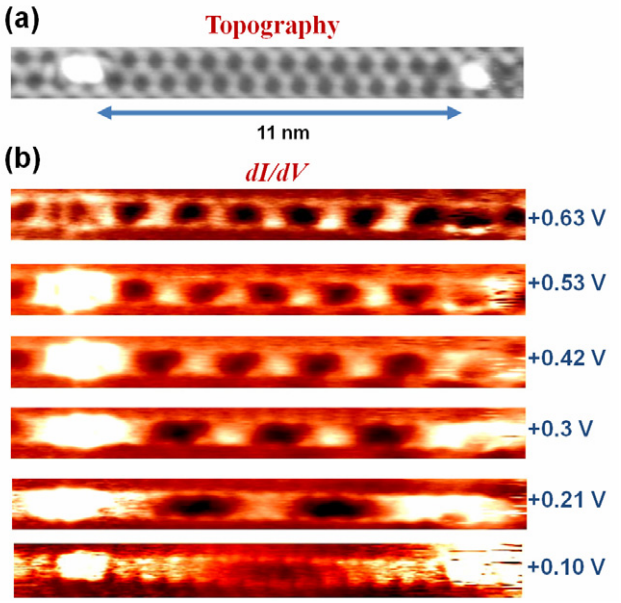

Figure 10. (a) STM topography image of Si(001) surface after deposition of two tungsten dots on a single dimer row to create an artificially fabricated quasi-1D quantum well. (b) Selected $\mathrm{d}I/\mathrm{d}V$ maps for different bias voltages obtained from quasi-1D quantum well (modulation of 20 mV at 6.5 kHz), which clearly shows several quantized states of confined electron waves.

STM nanofabrication method based on tip-material transfer by applying voltage pulses was introduced. The highly reproducible fabrication of metallic silver nanodots and nanowires using a silver-coated tip was demonstrated. The mechanism of tip-material transfer through the application of voltage pulses can be explained by the spontaneous formation of a point contact due to field-enhanced diffusion to the apex of the tip, for which most of the previous reports assigned field evaporation as being the dominant process. Secondly, another method of transferring STM tip material by applying *z*-direction pulses was introduced. Sub-nanometer displacement pulses along the *z*-direction (*z*-pulses) form point contacts resulting in reproducible nanodot deposition. Then, the discovery of the STM structural manipulation of surface phases was discussed. It was demonstrated that the superstructures on reconstructed Si(100) surfaces can be reverse-manipulated between the ground states and quasi-ground states by controlling the energy of the injected carriers. Finally, the fabrication of an atomic-scale 1D quantum confinement system was presented using a single-atom-deposition technique by controlling the point contact formation by the STM tip. Because of its combined nanofabrication and nanocharacterization capabilities, STM is a powerful tool for exploring the nanotechnology and nanoscience fields.

References

[1] Wiesendanger R 1994 *Scanning Probe Microscopy and Spectroscopy* (Cambridge: Cambridge University Press) p 542
[2] Fujita D 2002 *Materia Japan* **41** 623 (in Japanese)
[3] Fujita D 2004 *Nanotechnology* **15** Preface

[4] Binnig G, Rohrer H, Gerber Ch and Weibel E 1983 *Phys. Rev. Lett.* **50** 120
[5] Hamers R J, Tromp R M and Demuth J E 1986 *Phys. Rev. Lett.* **56** 1972
[6] Bode M, Getzlaff M and Wiesendanger R 1998 *Phys. Rev. Lett.* **81** 4256
[7] Stipe B C, Rezaei M A and Ho W 1998 *Science* **280** 1732
[8] Fujita D, Onishi K and Niori N 2004 *Microsc. Res. Tech.* **64** 403
[9] Crommie M F, Lutz C P and Eigler D M 1993 *Science* **262** 218
[10] McCord M A and Awschalom D D 1990 *Appl. Phys. Lett.* **57** 2153
[11] Matsumoto K, Ishii M, Segawa K and Oka Y 1996 *Appl. Phys. Lett.* **68** 34
[12] Schen T-C, Wang C, Lyding J W and Tucker J R 1995 *Appl. Phys. Lett.* **66** 976
[13] Mamin H J, Guethner P H and Ruger D 1990 *Phys. Rev. Lett.* **65** 2418
[14] Fujisawa T, Hirayama Y and Tarucha S 1994 *Appl. Phys. Lett.* **64** 2250
[15] Kamp M, Emmerling M, Kuhn S and Forchel A 1999 *J. Vac. Sci. Technol.* B **17** 86
[16] Rabe J P and Buchholz S 1991 *Appl. Phys. Lett.* **58** 702
[17] Pascual J I, Mendez J, Gomez-Herrero J, Baro A M, Garcia N and Binh V T 1993 *Phys. Rev. Lett.* **71** 1852
[18] Hsiao G S, Penner R M and Kingsley J 1993 *Appl. Phys. Lett.* **64** 1350
[19] Bessho K and Hashimoto S 1994 *Appl. Phys. Lett.* **65** 2142
[20] Chang C S, Su W B and Tsong T T 1994 *Phys. Rev. Lett.* **72** 574
[21] Radojkovic P, Schwartzkopff M, Enachescu M, Stefanov E, Hartmann E and Koch F 1996 *J. Vac. Sci. Technol.* B **14** 1229
[22] Chang T C, Chang, C S, Lin H N and Tsong T T 1994 *Appl. Phys. Lett.* **67** 903
[23] Fujita D, Jiang Q-D and Nejoh H 1996 *J. Vac. Sci. Technol.* B **14** 3413
[24] Fujita D, Jiang Q-D, Dong Z-C, Sheng H-Y and Nejoh H 1997 *Nanotechnology* **8** A10
[25] Huang D H, Nakayama T and Aono M 1998 *Appl. Phys. Lett.* **73** 3360
[26] Hu X and von Blanckenhagen P 1999 *J. Vac. Sci. Technol.* B **17** 265
[27] Park J Y and Phaneuf R J 2002 *J. Appl. Phys.* **92** 2139
[28] Fujita D and Kumakura T 2003 *Appl. Phys. Lett.* **82** 2329
[29] Abed H *et al* 2005 *J. Vac. Sci. Technol.* B **23** 1543
[30] Tsong T T 1991 *Phys. Rev.* B **44** 13703
[31] Fujita D, Dong Z-C, Sheng H-Y and Nejoh H. 1998 *Appl. Phys.* A **66** S753
[32] Takayanagi K, Tanishiro Y, Takahashi S and Takahashi M 1985 *Surf. Sci.* **164** 367
[33] Krans J M, Muller C J, Yanson I K, Movaert Th C M, Hesper R and Ruitenbeek J M 1993 *Phys. Rev.* B **48** 14721
[34] Olesen L, Laegsgaard E, Stengaard I, Besenbacher F, Schiotz J, Stoltze P, Jacobsen K W and Norskov J K 1994 *Phys. Rev. Lett.* **72** 2251
[35] Stalder A and Durig U 1996 *J. Vac. Sci. Technol.* B **14** 1259
[36] Kondo Y, Amakusa T, Iwatsuki M and Tokumoto H 2000 *Surf. Sci.* **453** L318
[37] Yokoyama T and Takayanagi K 2000 *Phys. Rev.* B **61** 5078
[38] Matsumoto M, Fukutani K and Okano T 2003 *Phys. Rev. Lett.* **90** 106103
[39] Hata K, Yoshida S and Shigekawa H 2002 *Phys. Rev. Lett.* **89** 286104
[40] Sagisaka K, Fujita D and Kido G 2003 *Phys. Rev. Lett.* **91** 146103
[41] Sagisaka K, Kitahara M and Fujita D 2003 *Japan. J. Appl. Phys.* **42** L126
[42] Uozumi T, Tomiyoshi Y, Suehiro N, Sugawara Y and Morita S 2002 *Appl. Surf. Sci.* **188** 279
[43] Sagisaka K, Kitahara M, Fujita D, Kido G and Koguchi N 2004 *Nanotechnology.* **15** S371
[44] Mizuno S, Shirasawa T, Shiraishi Y and Tochihara H 2004 *Phys. Rev.* B **69** 241306
[45] Ramstad A, Brocks G and Kelly P J 1995 *Phys. Rev.* B **51** 14504
[46] Sagisaka K, Fujita D, Kido G and Koguchi N 2004 *Surf. Sci.* **566–568** 767
[47] Johansson L S O and Reihl B 1992 *Surf. Sci.* **269–270** 810
[48] Northrup J E 1993 *Phys. Rev.* B **47** 10032
[49] Sagisaka K and Fujita D 2005 *Phys. Rev.* B **71** 245319
[50] Takagi Y, Yoshimoto Y, Nakatsuji K and Komori F 2003 *J. Phys. Soc. Japan* **72** 2425
[51] Yokoyama T and Takayanagi K 1999 *Phys. Rev.* B **59** 12232
[52] Sagisaka K and Fujita D 2005 *Phys. Rev.* B **72** 235327
[53] Sagisaka K and Fujita D 2006 *Appl. Phys. Lett.* **88** 2031118